Digital Signal Processing 20 (2010) 1579–1591

Contents lists available at ScienceDirect

Digital Signal Processing

www.elsevier.com/locate/dsp

Automated study of ocular thermal images: Comprehensive analysis of corneal health with different age group subjects and validation

Jen-Hong Tan [a], E.Y.K. Ng [a,*], Rajendra Acharya U [b], C. Chee [c]

[a] School of Mechanical and Aerospace Engineering, College of Engineering, Nanyang Technological University, 50, Nanyang Avenue, Singapore 639798
[b] Department of Electronics and Computer Engineering, Ngee Ann Polytechnic, Singapore
[c] Medical & Surgical Retinal Centre Department of Ophthalmology, National University Hospital, Singapore 119074

ARTICLE INFO

Article history:
Available online 30 March 2010

Keywords:
Infrared
Thermogram
Target tracing function
Snake
Cornea
Genetic algorithm

ABSTRACT

Thermography using infrared (IR) imaging is a non-invasive imaging technique widely used in medical and engineering arena nowadays. This technique is capable of detecting temperature changes in the vascular tissues, and plays an important role in the study of ocular surface temperature and ocular diseases. In this study the performance of an automated algorithm which acquires corneal surface temperature was studied for normal IR thermograms of different age groups. The automated algorithm consists of algorithms intelligently localizing cornea and removing eye lashes, reading in temperature values within the localized cornea without any human intervention for further analysis. Its performance was compared against the results of manual corneal delineation. Our studies showed that the automated algorithm performed as good as the tedious and laborious manual method with the calculated average corneal temperature of $34.01 \pm 0.64\,^{\circ}C$ (automated) and $33.99 \pm 0.63\,^{\circ}C$ for manual method.

1. Introduction

Any object, when its temperature is above absolute zero Kelvin, emits electromagnetic radiations that are invisible to human eye when the object temperature is not too high. Infrared thermography allows one to see the thermal energy over the surfaces of some objects. Over the past 50 years, infrared thermography has been applied for the purpose of condition monitoring, preventive maintenance, thermal building survey and medical diagnosis.

Nowadays, in medical field human body temperature is often used as one of the diagnostic indicator or marker to identify some diseases. With the advent of color coded infrared (IR) thermal imaging, body temperature has been used and applied for the detection of rheumatism [1], breast cancer [2], skin lesion [3] and impotence [4].

Ocular surface temperature (OST) can be used to diagnose ocular disease, with the aid of thermal imaging. In the past, OST was measured invasively to detect the health of a subject's eye [5]. Later, Mapstone used bolometer to study OST by measuring the amount of IR radiated from eye [6]. Subsequently, IR thermal imaging was employed in medical field for the diagnosis of different diseases [7]. These days, they are used in the ophthalmology to study OST [7–9].

Despite the advances in technology of capturing IR and displaying thermal distribution, the study of OST is still an issue in several situations due to the unclear thermal boundary in between iris and sclera when compared to optical image. Hence, the localization of cornea is a difficult problem, and may lead to inconsistency in studying the corneal surface temperature. Researchers usually overcome this problem by manually locating the cornea, as the automated localization of eye and cornea is not straightforward.

* Corresponding author: Adjunct NUH Scientist, Office of Biomedical Research, National University Hospital of Singapore. Fax: +65 67911859.
E-mail address: mykng@ntu.edu.sg (E.Y.K. Ng).

1051-2004/$ – see front matter
doi:10.1016/j.dsp.2010.03.014

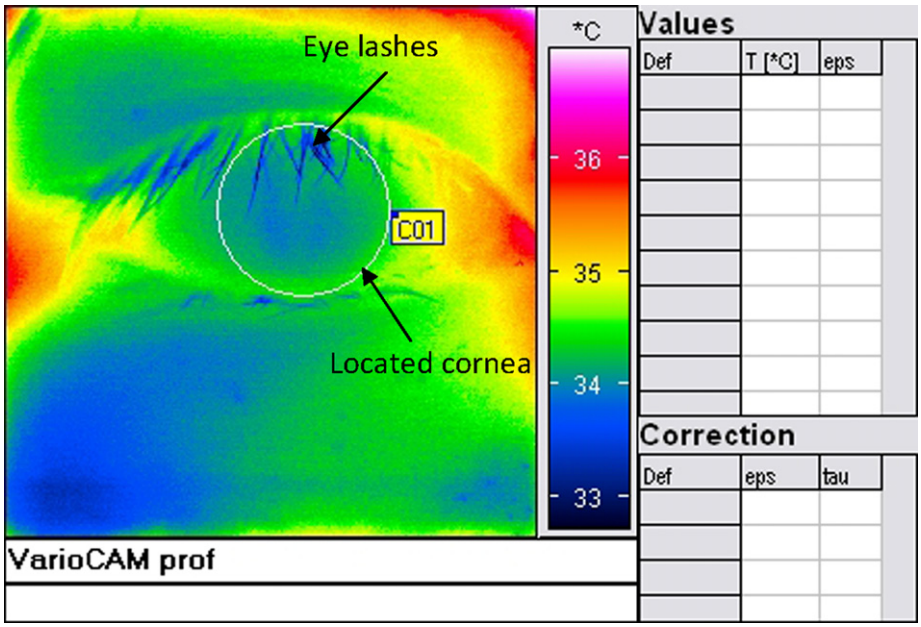

Fig. 1. Typical IR thermogram of a normal subject.

Efron et al. have studied the OST by estimating the geometric center of cornea, and measured surface temperature for every 0.5 mm increments on either side of corneal surface horizontally [10]. Morgan et al. have used average temperature for the analysis by placing five 10×10 pixels boxes on the estimated geometric center of cornea, limbal position, temporal and nasal conjunctiva (2 mm from the limbus) respectively [11]. Central corneal surface temperature was determined by placing a 10×10 pixels box on the estimated geometric center of cornea, and thus the mean temperature was obtained to study the relationship between corneal surface temperature and the age [12]. The effect of contact lens wear on corneal surface was studied using the thermal values of the 23 points on the anterior portion of the eye [13].

It can be seen from the above mentioned studies that in the past corneal temperature was vaguely determined. Recently, the corneal temperature was studied within a circular shape closed to the actual cornea, where the size of diameter and the position of that circle were estimated manually [9]. They have reported an average corneal surface temperature of 35.07 °C and 35.18 °C for left and right eyes respectively.

OST is sensitive to external conditions. In addition to pathophysiology, exposure of eye to air, environmental conditions such as humidity and temperature, blinking of the eye lid and the presence of contact lens may also affect OST readings. Hence often in the study of OST, factors such as blinking, humidity, environment temperature and contact lens are tightly controlled in order to achieve reasonable accuracy.

Early in 1960s, an average corneal temperature of 34.8 °C was reported considering the effect of blinking and tears, and several ocular diseases such as anterior uveitis, iridocyclitis, carotid artery disease and posterior segment pathology were also investigated [14]. Anterior segment of eye infected with inflammation was determined to have higher OST compared to normal eye in later investigations [15].

For normal subjects, the average corneal temperature was reported to be 35.4 ± 0.1 °C by Petrou [16]. He observed specific patterns in thermograms of iridocyclitis and normal eye. He showed that subjects with iridocyclitis had a “hot ring” on the cornea above the ciliary body, and corneal temperatures in these cases were 2.2 °C higher than normal subjects. It was also noted that a temperature difference of up to 3 °C between a pair of eyes in which one eye had undergone cataract surgery and the other had cataract eye [16].

A difference of 0.45 °C was observed between central corneal and limbus temperature for normal subjects by Morgan et al. [10,11]. Corneal temperature was documented to decrease at a rate of 0.001 °C per year with age, though the relationship between age and OST was not significant [12]. The difference in corneal surface temperature between two eyes was less than 0.6 °C for most of the normal population [11].

Recently, for normal subjects the average corneal temperature was reported to be 35.4 ± 0.1 °C by Petrou [16]. He observed specific patterns in thermograms of iridocyclitis and normal eye. He showed that subjects with iridocyclitis had a “hot ring” on the cornea above the ciliary body, and corneal temperatures in these cases were 2.2 °C higher than normal subjects. It was also noted that a temperature difference of up to 3 °C between a pair of eyes in which one eye had undergone cataract surgery and the other had cataract eye [16].

So far, there is no technique reported on the automated localization of eye and cornea. A semi-automated technique was recently developed and used to localize cornea and obtain average OST within cornea [8]. It showed that OST decreased with age. In current work, OST of normal subjects were studied by employing an algorithm which was fully automated in

Table 1
Age groups of this study.

Age group	Number of subjects
Below 30	32
30–50	19
After 50	16
Total	67

the localization of eye [17,18]. Furthermore eye lashes that fell on eye were removed to increase accuracy in the acquired OST. Fig. 1 shows the typical IR thermogram of the normal eye. It can be seen that there are eye lashes falling on the eye and the temperatures of eye lashes are much lower as compared to the OST. Hence, to achieve considerable accuracy in getting temperatures close to the actual OST, these eye lashes are to be removed. The removal of eyelashes involves steps of normalizing image, Gabor filtering, and expectation-maximization (EM) algorithm to estimate the Gaussian mixture. The performance of the automated cornea localization method after removing the eye lashes was compared with the manual method, and OST of different age group of normal subjects was evaluated using both methods.

The layout of this paper is as follow: Section 2 presents the data acquisition process. Sections 3 and 4 explain the methods used and the results of both methods of corneal localization respectively. Discussion on results of both methods is presented in Section 5 and finally the paper concludes in Section 6.

2. Data acquisition

The thermograms used in this study are taken from normal subjects with age ranging from 14 to 68, as summarized in Table 1. Before data collection, subjects were requested to relax for 10 minutes. During data acquisition, subjects were not allowed to blink a few seconds before a shot, and could only blink after the shot is taken. Special care was taken to exclude participants with the following conditions:

I. Hot drinks, rubbing of eyes, use of tear drops.
II. Current eye disease.
III. History of serious eye disease.
IV. History of ocular or facial surgery.
V. Poor general health.
VI. Recent usage of tear drop or medications.
VII. Wearing of contact lens.

VarioCAM, JENOPTIK Laser (Germany) (URL: http://www.jenoptik-ir.com/) was used to capture infrared images and images were placed 50 cm away from chin-rest. Thermogram was obtained in controlled environmental conditions where temperature was maintained at $25 \pm 1\,^{\circ}\mathrm{C}$ and a mean humidity of 84%. All the images taken are stored in *irbis* format. These *irbis* data were exported to *jpeg* format with an image size of 256×256 pixels using post-processing software installed with the camera.

Data collection was conducted at Biomedical Centre, Ngee Ann Polytechnic, Singapore.

3. Methods used

3.1. Manual localization of cornea

Manual localization of cornea was carried out using a built-in software IRBIS plus 2.2 provided by Jenoptik. Temperature values are displayed in RGB colors in the program, and a circle was drawn close to the cornea [8]. Average, minimum, maximum and spanning temperature within the circular region are evaluated by the software as shown in Fig. 2.

3.2. Automated method of studying corneal surface temperature

This step involves the localization of cornea and removal of eye lashes. They are explained in the following sections.

3.2.1. Localization of eye and cornea

The automated localization of eye and cornea was achieved using snake algorithm and target tracing function coupled with genetic algorithm [17,18], as illustrated in Fig. 3. Snake [19] is an active contour consisting a series of points (dubbed snake points) moving under gradient vector flow (GVF) [20] force field to lock onto nearby edges. Hence, it delineates the shape of an eye accurately provided the initial contour is of correct shape and put closed to the eye. Target tracing function is adopted to overcome the problem accompanied with the initialization of snake algorithm, and the search for minimum on that function was solved by genetic algorithm. As snake correctly converges into and encloses ocular region, the corneal radius and its center position were located based on the resultant snake points.

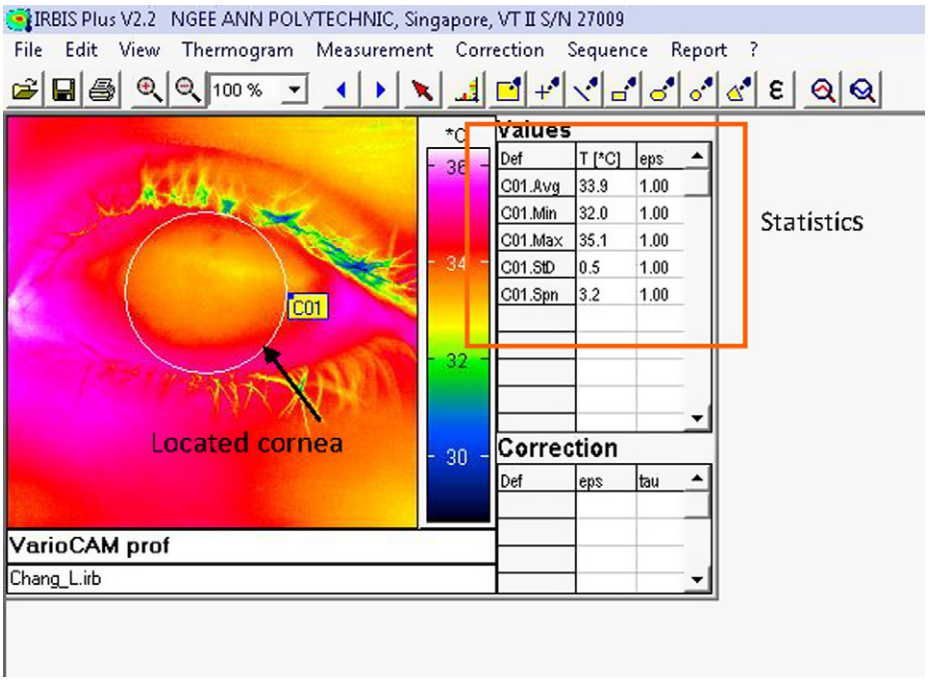

Fig. 2. Method of manual localization of cornea.

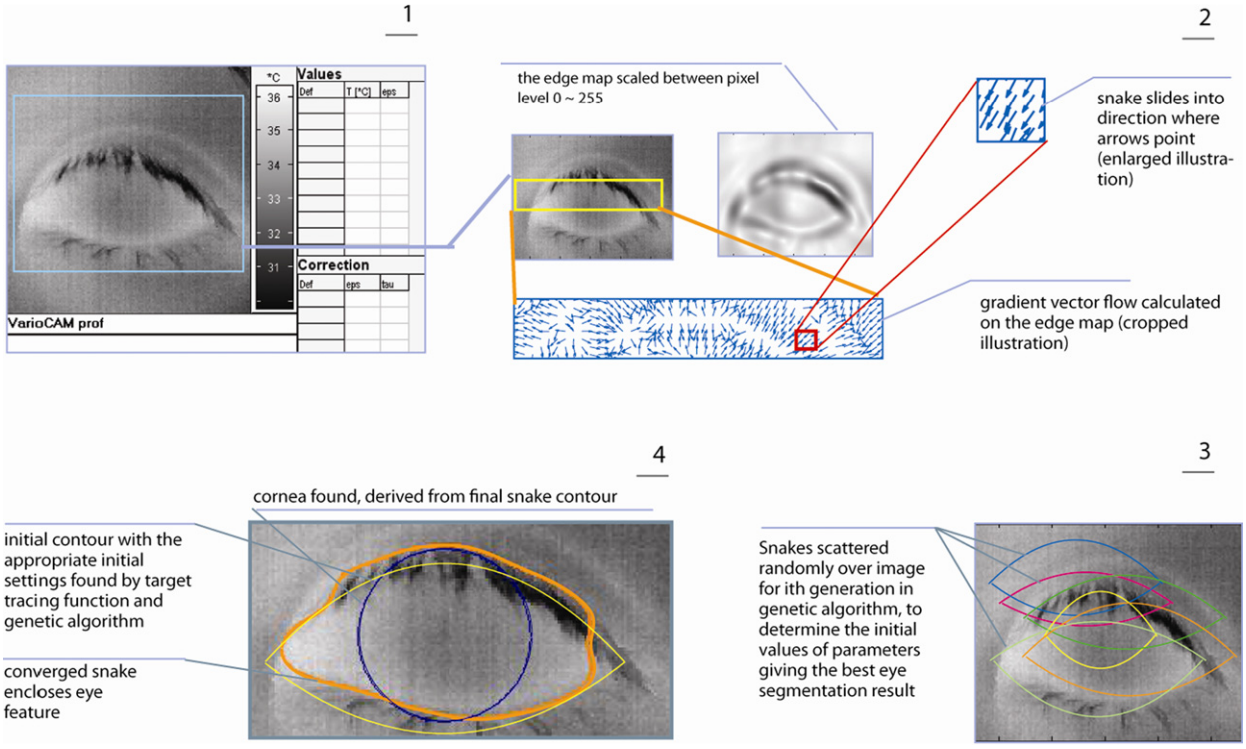

Fig. 3. Automated of localization of eye and cornea.

3.2.1.1. Snake and gradient vector flow Snake is a curve $\mathbf{x}(s) = [x(s) \quad y(s)]$, $s \in [0, 1]$ defined over an image domain [19], and moves through the image spatial domain under a combination of forces to minimize the energy functional

$$E = \int_0^1 \frac{1}{2}\left[\alpha\left|\mathbf{x}'(s)\right|^2 + \beta\left|\mathbf{x}''(s)\right|^2\right] + E_{ext}\left(\mathbf{x}(s)\right) ds \tag{1}$$

The solution to the above functional is given by

$$\begin{cases} x_t = (A + \gamma I)^{-1}(\gamma x_{t-1} - f_x(x_{t-1}, y_{t-1})) \\ y_t = (A + \gamma I)^{-1}(\gamma y_{t-1} - f_y(x_{t-1}, y_{t-1})) \end{cases} \tag{2}$$

where α and β are parameters that control the snake length and rigidity [20], $\mathbf{x}'(s)$ and $\mathbf{x}''(s)$ are the first and second derivatives with respect to s, the contour's parameter. A is a pentadiagonal banded matrix, γ is step-size and $\nabla E_{ext} = [f_x(x, y) \quad f_y(x, y)]$. E_{ext} refers to the external force that pushes snake toward smaller value in its total energy. In this study we use gradient vector flow (GVF) field as external energy function: $E_{ext} = \mathbf{v}(x, y) = [u(x, y), v(x, y)]$. GVF is a dense vector field that minimizes the functional

$$\varepsilon = \iint \mu\left(u_x^2 + u_y^2 + v_x^2 + v_y^2\right) + |\nabla f_e|^2 |\mathbf{v} - \nabla f_e|^2 \, dx\, dy \tag{3}$$

where μ is a parameter regularizing the first term and the second term in integrand; $f_e(x, y)$ is the edge map, in this study it is defined as

$$f_e = -\left\{\left|\nabla\left[G_{\sigma_1}(x, y) * I(x, y)\right]\right| + r_e \cdot G_{\sigma_2}(x, y) * \left|\nabla_{sob} I(x, y)\right|\right\} \tag{4}$$

in which r_e is a control parameter; ∇_{sob} is the Sobel gradient operator. G_{σ_1} and G_{σ_2} are Gaussian blur functions having standard deviations of σ_1 and σ_2 respectively [17,18]. The proposed edge map combines two sort of external forces, which have slight difference in between one another, to smoothen image and preserve subtle pixel difference in the region of lower eyelid within the ocular thermo image [17,18].

In the actual implementation of GVF snake, it was found that snake often gets trapped in image border, due to artifacts introduced during calculation of Gaussian blur and GVF force field [17,18]. This problem is resolved by expanding image matrix, through a number of iterative calculations. Let A be an image matrix with a size of $m \times n$, the expanded image after each iteration is matrix B, having the size of $(m + 2) \times (n + 2)$ [17,18]:

$$A = \begin{bmatrix} a_{1,1} & a_{1,2} & \cdots & a_{1,n} \\ a_{2,1} & a_{2,2} & \cdots & a_{2,n} \\ \vdots & \vdots & \ddots & \vdots \\ a_{m,1} & a_{m,2} & \cdots & a_{m,n} \end{bmatrix}, \qquad B = \begin{bmatrix} b_{1,1} & b_{1,2} & \cdots & b_{1,n+1} & b_{1,n+2} \\ b_{2,1} & b_{2,2} & \cdots & b_{2,n+1} & b_{2,n+2} \\ \vdots & \vdots & \ddots & \vdots & \vdots \\ b_{m+1,1} & b_{m+1,2} & \cdots & b_{m+1,n+1} & b_{m+1,n+2} \\ b_{m+2,1} & b_{m+2,2} & \cdots & b_{m+2,n+1} & b_{m+2,n+2} \end{bmatrix}$$

Then:

$$\begin{cases} (b_{i,j})_{2 \leqslant i \leqslant m+1;\, 2 \leqslant j \leqslant n+1} = (a_{i,j})_{1 \leqslant i \leqslant m;\, 1 \leqslant j \leqslant n} \\ b_{1,j} = a_{1,j-1} - \mu\left(a_{1,j-1} - \frac{a_{1,1} + a_{1,2} + \cdots + a_{1,n}}{n}\right), \quad \text{for } j = 2, 3, \ldots, n+1 \\ b_{m+2,j} = a_{m,j-1} - \mu\left(a_{m,j-1} - \frac{a_{m,1} + a_{m,2} + \cdots + a_{m,n}}{n}\right), \quad \text{for } j = 2, 3, \ldots, n+1 \\ b_{i,1} = a_{i-1,1} - \mu\left(a_{i-1,1} - \frac{a_{1,1} + a_{2,1} + \cdots + a_{m,1}}{m}\right), \quad \text{for } i = 2, 3, \ldots, m+1 \\ b_{i,n+2} = a_{i-1,n} - \mu\left(a_{i-1,n} - \frac{a_{1,n} + a_{2,n} + \cdots + a_{m,n}}{m}\right), \quad \text{for } i = 2, 3, \ldots, m+1 \\ b_{1,1} = \frac{b_{1,2} + b_{2,1}}{2}, \quad b_{1,n+2} = \frac{b_{1,n+1} + b_{2,n+2}}{2}, \quad b_{m+2,1} = \frac{b_{m+1,1} + b_{m+2,2}}{2}, \quad b_{m+2,n+2} = \frac{b_{m+1,n+2} + b_{m+2,n+1}}{2} \end{cases} \tag{5}$$

3.2.1.2. Target tracing function and genetic algorithm The initial contour consists of two parabolas [17,18], as illustrated in Fig. 4. The initial contour can be generated by

$$\mathbf{C}(x_c, y_c, p_1, p_2, w) = \left[C_u(s) \quad C_l(s)\right]^T = \mathbf{C}(s) \tag{6}$$

where

$$\begin{cases} C_u(s) = [y_u(s) \quad x_u(s)] = \left[\frac{(x_u(s) - x_c)^2}{-4p_1 w} + (y_c + p_1 w) - h_u \quad x_u(s)\right], \quad \text{for } 0 < s \leqslant 0.5 \\ C_l(s) = [y_l(s) \quad x_l(s)] = \left[\frac{(x_l(s) - x_c)^2}{4p_2 w} + (y_c - p_2 w) - h_l \quad x_l(s)\right], \quad \text{for } 0.5 < s < 1 \end{cases}$$

and

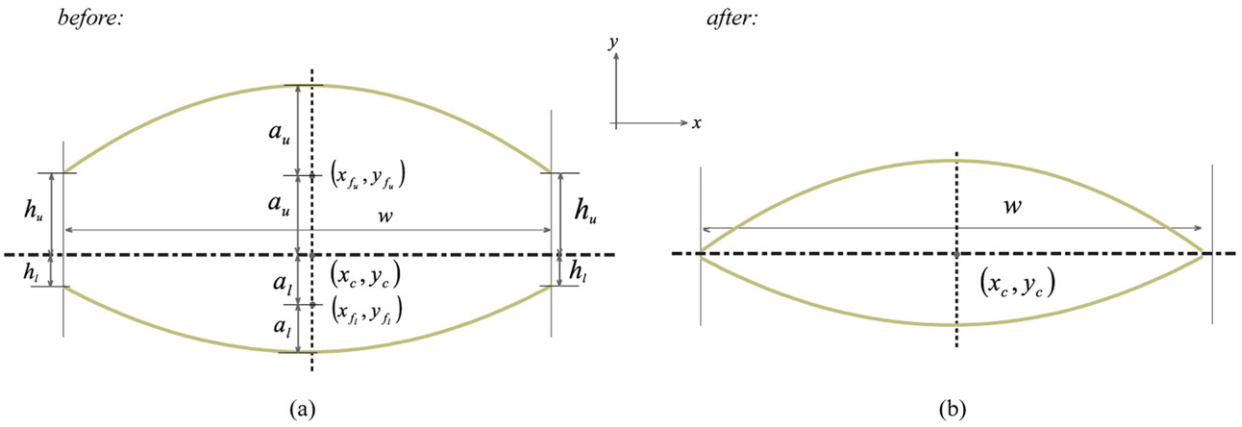

Fig. 4. (a) Setup of parabola for initial contour; (b) final look of initial contour.

$$p_1 = \frac{a_u}{w}, \qquad p_2 = \frac{a_l}{w}$$

$$h_u = \frac{(x_c - w/2)^2}{-4p_1 w} + (y_c + p_1 w), \qquad h_l = \frac{(x_c - w/2)^2}{4p_2 w} + (y_c - p_2 w)$$

$\mathbf{C}(s)$ is a series of snake points, which is in fact $\mathbf{x}(s) = [x(s) \quad y(s)]$ in discrete form. These points undergo deformation through Eq. (2) until (1) reaches minimum. After each iteration a step of equal-distant redistribution of points is followed to speed up convergence time. Let ${}^{v}\mathbf{C}(s) = {}^{v}\mathbf{C}(x_c, y_c, p_1, p_2, w)$ denotes the converged snake deformed from initial contour $\mathbf{C}(s) = \mathbf{C}(x_c, y_c, p_1, p_2, w)$, the target tracing function is defined as [17,18]:

$$y_{ft} = F_{tt}(x_c, y_c, p_1, p_2, w) = \int \left[\left\| \frac{d^2}{ds^2} I_{sc}\left({}^{v}\mathbf{C}(s)\right) \right\| \times c_1 + I_{sc}^2\left({}^{v}\mathbf{C}(s)\right) + \left| {}^{v}\mathbf{C}'(s) \right| \times c_2 \right] ds + c_3 \times \frac{\int_0^1 I_{sc}^2({}^{v}\mathbf{C}(s))\, ds}{\int_0^1 |{}^{v}\mathbf{C}'(s)|\, ds} \tag{7}$$

in which

$$I_{sc} = \frac{f_e(x, y) - \min f_e}{\max f_e - \min f_e}, \qquad \frac{d^2}{ds^2} I_{sc}\left({}^{v}\mathbf{C}(s_n)\right) \approx I_{sc}\left({}^{v}\mathbf{C}(s_{n+1})\right) - 2I_{sc}\left({}^{v}\mathbf{C}(s_n)\right) - I_{sc}\left({}^{v}\mathbf{C}(s_{n-1})\right)$$

where f_e refers to the edge map defined in Eq. (4), and I_{sc} is the f_e scaled in the range of 0–1. c_1, c_2, c_3 are control parameters. The ${}^{v}\mathbf{C}(s)$ that gives the lowest value in target tracing function corresponds to the converged snake accurately localizing the eye of interest. A search for minimum is performed on target tracing function over variables x_c, y_c, p_1, p_c and w, and in the proposed method, genetic algorithm is opted to perform the search.

Genetic algorithm is a stochastic search technique widely used in computing exact or approximate solution to optimization problem, or for the search of global minima. It starts with a population (the first generation) with a fixed number of individuals generated at random. Each individual within the population is denoted by a chromosome, representing one of the potential solutions to the problem, and in each generation the fitness of each individual is evaluated using target tracing function. Through procedures of selection (i.e. individuals with better fitness are more likely to be reproduced in the next generation), reproduction, crossover, mutation, these individuals evolve generation by generation on the basis of "survival of the fittest". These procedures run iteratively until the best fit individual is found.

In our genetic algorithm, values of x_c, y_c, p_1, p_c and w were encoded in chromosome, denoting a single initial contour (individual). At first generation, initial contours were generated at random through Eq. (6). These initial contours span over the spatial domain of the image of interest, with various values in p_1, p_c and w. After that, each of the initial contours converges (by Eq. (1)) under the GVF force field, becoming a converged snake. The converged snake was then evaluated using target tracing function (Eq. (7)) to determine the fitness of this entity. If a converged snake was fit enough to compete against the other peers and survives under the procedures of selection, it was very likely that its chromosome (which consists of the values of x_c, y_c, p_1, p_c and w) will be passed down and crossed over to form a more competitive chromosome (individual). The resultant chromosome will again appear as an initial contour in a new generation, converge under external force field and going through once again the procedures of evaluation, selection, reproduction crossover and mutation. The algorithm runs generation by generation until there is a snake that can accurately delineate the eye is found.

3.2.1.3. Locating cornea The cornea is assumed to be a circle, and since snake points ${}^{v}\mathbf{C}(s) = [{}^{x}C(s) \quad {}^{y}C(s)]$ are equi-distant, its center can be obtained through

$$\begin{cases} x_{cc} = \frac{1}{n_s} \sum_s {}^x C(s) \\ y_{cc} = \frac{1}{n_s} \sum_s {}^y C(s) \end{cases} \tag{8}$$

where n_s denotes the total number of snake points. Let the radius of cornea be r_c, then

$$r_c = rt \times dX \tag{9}$$

Define

$$dX = \max {}^x C(s) - \min {}^x C(s) \tag{10}$$

$$dY = \max {}^y C(s) - \min {}^y C(s) \tag{11}$$

For a snake that correctly converges to the edge of an eye, its dX and dY as defined above are almost equal to the width and the height of the eye. Corneal radius was said to be approximately about 0.25 times of the width of an eye [21], so the dX/dY for an eye would be 2 (assume the cornea touches the upper and lower eyelid). And rt is 0.25 in this case for Eq. (9) to be true.

When a snake only converges to the edge of cornea, in this case the dX/dY is 1 since cornea is assumed to be circular, and rt is 0.5 for Eq. (9) to be true. From these two cases we propose a formula to adaptively determine the corneal radius solely from the points of a converged snake. Based on simple interpolation

$$\frac{2-1}{0.25-0.5} = \frac{\frac{dX}{dY} - 1}{rt - 0.5}$$

Hence

$$rt = \left(\frac{dX}{dY} - 1\right)(-0.25) + 0.5 \tag{12}$$

With rt known, the corneal radius r_c can be determined through Eq. (9). As the size of an eye varies among individuals, the above formulation allows the algorithm to adaptively determine the size of cornea on the basis of the shape of a snake, as long as the snake correctly localizes the eye.

3.2.2. Removal of eye lashes

Alonso-Caneiro et al. have estimated corneal surface topography with videokeratoscopy, by identifying strong interference signal due to factors such as narrow palpebral apertures, nystagmus and long eyelashes [22]. We have modified this technique for the identification of eyelashes in the IR thermogram. Temperature data of eye lashes were removed or avoided in an automated fashion with locations of eye lashes identified using the modified technique.

After the ocular localization our algorithm generated a square matrix, the width of which was the size of corneal diameter. The square matrix was resized to 300×300 pixels after using linear interpolation to give a better identification of eye lashes (usually the size of square matrix before resize is not more than 100×100 pixels). Then a series of concentric rings were superimposed to the resized square matrix. The details of image superposition and the following procedures are illustrated in steps below.

3.2.2.1. Superposition of concentric rings The center of concentric rings coincides with the center of resized square matrix, and each of the stripes (or ring) has a width of 2.8 pixels. Fig. 5 shows the concentric rings of bright and dark stripes alternatively. The pixels in regions of brighter stripes, has an intensity level 0.04 higher compared to the same region before superposition; and for pixels in regions of darker stripes, their intensity level are 0.04 lower compared to the same region before superposition (at this stage of processing, value of 0 corresponds to the darkest and value of 1 corresponds to the brightest pixel intensity level). The width of one bright stripe and one dark stripe combined forms the wavelength in terms of Gabor filter processing.

3.2.2.2. Normalization The superimposed image forms a 2D matrix $I[n, m]$, with $n = 1, 2, \ldots, N$ and $m = 1, 2, \ldots M$, and is divided into non-overlapped blocks of equal size. Let W denote block width and $\lfloor \cdot \rfloor$ as floor operator, for an image block centered at $[n_b, m_b]$:

$$I_{\text{block}} = \begin{bmatrix} \left[n_b - \frac{W}{2} + 1, m_b - \frac{W}{2} + 1\right] & \cdots & \left[n_b, m_b - \frac{W}{2} + 1\right] & \cdots & \left[n_b + \frac{W}{2}, m_b - \frac{W}{2} + 1\right] \\ \vdots & \ddots & & \ddots & \\ \left[n_b - \frac{W}{2}, m_b\right] & \cdots & \left[n_b, m_b\right] & \cdots & \left[n_b + \frac{W}{2}, m_b\right] \\ \vdots & \ddots & & \ddots & \\ \left[n_b - \frac{W}{2} + 1, m_b - \frac{W}{2}\right] & \cdots & \left[n_b, m_b + \frac{W}{2}\right] & \cdots & \left[n_b + \frac{W}{2}, m_b + \frac{W}{2}\right] \end{bmatrix} \tag{13}$$

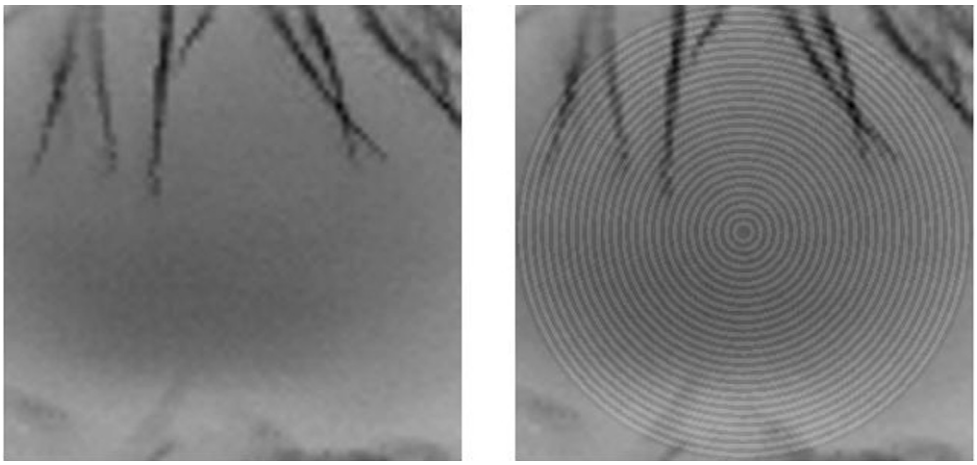

Fig. 5. Square matrix (a) before superposition and (b) after superposition.

where

$$n_b = \frac{W}{2}, \frac{W}{2} + W, \frac{W}{2} + 2W, \ldots, \frac{W}{2} + \left(\left\lfloor \frac{N}{W} \right\rfloor - 1\right)W$$

$$m_b = \frac{W}{2}, \frac{W}{2} + W, \frac{W}{2} + 2W, \ldots, \frac{W}{2} + \left(\left\lfloor \frac{M}{W} \right\rfloor - 1\right)W$$

The block size in this study is set to 6×6 pixels, since the width of stripe is 2.8 pixels, such size of block is sufficient to contain information for identification of eye lashes. Statistical block normalization with zero mean and unit variance is applied to remove background, in order to ensure further image processing is not affected by the variation of temperatures in thermogram.

3.2.2.3. Gabor filtering A Gabor filter is defined as

$$f(n, m; \theta, \sigma_n, \sigma_m) = \exp\left[-\frac{1}{2}\left(\frac{R_1^2}{\sigma_n^2} + \frac{R_2^2}{\sigma_m^2}\right)\right] \cdot \exp\left(i\frac{2\pi R_1}{\lambda}\right) \tag{14}$$

where

$$R_1 = n\cos\theta + m\sin\theta, \qquad R_2 = -n\sin\theta + m\cos\theta$$

θ and λ are the orientation and the wavelength of sinusoidal wave respectively; σ_n and σ_m are standard deviations for Gaussian function along n and m axes.

Gabor filter in this technique is used to determine if an area on the image had a specific orientation. The presence of interference such as eye lashes often associates with no specific orientation in an area after Gabor filter processing. In other words, given an image convoluted with a bank of Gabor filter having K different orientations, outputs of all these filters would give similar values for regions where eye lashes were present [22].

Thus, Eq. (14) is rewritten to obtain output of k-th Gabor filter

$$g(n, m; \theta_k, \lambda, \sigma_n, \sigma_m) = I[n, m] * f(n, m; \theta_k, \lambda, \sigma_n, \sigma_m) \tag{15}$$

The block sample mean of each of the filter outputs is given by

$$G_k = \frac{1}{W^2}\sum_{n_b}\sum_{m_b} g_{\text{block}}(n_b, m_b; \theta_k, \lambda, \sigma_n, \sigma_m) \tag{16}$$

in which $g_{\text{block}}(n_b, m_b)$ is part of the filter output of (3) corresponding to $I_{\text{block}}(n_b, m_b)$. For each image block we could get a vector $\mathbf{G} = [G_1, G_2, \ldots, G_k]$ and derive the sample standard deviation for the vector $\mathbf{G}$, $\hat{s}[n_b, m_b]$ [22]. In the presence of eye lashes, the value of the sample standard deviation of the vector $\mathbf{G}$ would be low since the filter outputs of different orientation provide similar values.

In this study $K = 8$ is selected for Gabor filter, and the value of λ is set to 5.6, the width of bright and dark stripes combined. $\sigma_n = \sigma_m$ is chosen since the rings pattern is regular and consistent, and the values of both are fixed at 0.5λ in order to achieve a good localization of eye lashes [22].

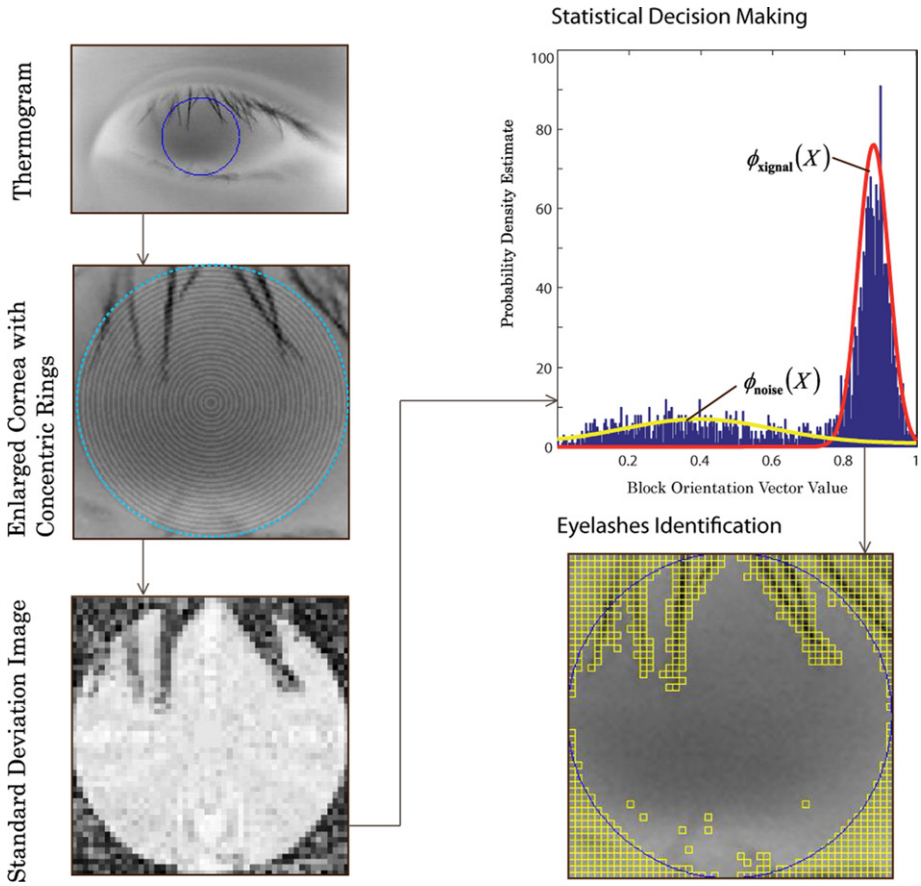

Fig. 6. Steps of removal of eye lashes.

3.2.2.4. Image segmentation After Gabor filtering, the matrix $\hat{s}[n_b, m_b]$ is normalized into range of 0 (non-oriented pattern) to 1 (maximally oriented pattern). All the columns of the normalized matrix are concatenated to form the block orientation vector, and the probability density function of this vector shows a bimodal distribution which can be approximately modeled as Gaussian mixture:

$$\phi\big(x[n];\varepsilon\big) = (1-\varepsilon)\phi_{\text{signal}}(X) + \varepsilon\phi_{\text{noise}}(X) \tag{17}$$

in which ε is the mixture parameter, and $0 < \varepsilon < 1$; ϕ_{signal} and ϕ_{noise} correspond to the Gaussian probability density functions of the oriented and non-oriented blocks [22].

The values of parameters of the Gaussian mixture $\hat{\mu}_{\text{signal}}, \hat{\sigma}_{\text{signal}}, \hat{\mu}_{\text{noise}}, \hat{\sigma}_{\text{noise}}$ are estimated using expectation-maximization (EM) algorithm [23]. Then the threshold is used to distinguish between areas of interference (eye lashes) and areas of corneal surface, is set to $\hat{\mu}_{\text{signal}} - 3\hat{\sigma}_{\text{signal}}$ as suggested [22]. Thus, for blocks having sample standard deviation of vector **G** lower than $\hat{\mu}_{\text{signal}} - 3\hat{\sigma}_{\text{signal}}$ are identified as interference. The entire procedure is illustrated in Fig. 6.

3.2.2.5. Estimation of removal effects of eyelashes The introduction of eyelashes removal has prevented reading in of temperatures which are lower in nature compared to corneal surface temperature. The effect of this introduction can be estimated with the use of two statistics. For a study which has a number N_c of corneas, *Mn* and *Mx* are the minimum and maximum temperature of *n*-th cornea, then we have

$$D_{Mn} = \frac{1}{N_c}\sum_{i=1}^{N_c} |Mn_{m_i} - Mn_{a_i}| \tag{18}$$

and

$$D_{Mx} = \frac{1}{N_c}\sum_{i=1}^{N_c} |Mx_{m_i} - Mx_{a_i}| \tag{19}$$

where subscripts *m* and *a* stand for manual and automated corneal localization methods respectively.

Table 2
Basic statistics of all subjects.

Parameters	Automated	Manual
Average corneal temperature	$34.01 \pm 0.64\,^{\circ}C$	$33.99 \pm 0.63\,^{\circ}C$
Standard deviation of temperatures within localized cornea	$0.24 \pm 0.08\,^{\circ}C$	$0.24 \pm 0.10\,^{\circ}C$
Left–right eye average corneal temperature difference	$0.22 \pm 0.21\,^{\circ}C$	$0.21 \pm 0.18\,^{\circ}C$

Table 3
Basic statistics on each age group.

Parameters	Age groups	Automated	Manual
Average corneal temperature	Below 30	$34.19 \pm 0.66\,^{\circ}C$	$34.15 \pm 0.68\,^{\circ}C$
	30–50	$33.88 \pm 0.61\,^{\circ}C$	$33.88 \pm 0.58\,^{\circ}C$
	After 50	$33.82 \pm 0.51\,^{\circ}C$	$33.81 \pm 0.47\,^{\circ}C$
Standard deviation of temperatures within localized cornea (average)	Below 30	$0.24 \pm 0.08\,^{\circ}C$	$0.24 \pm 0.09\,^{\circ}C$
	30–50	$0.24 \pm 0.08\,^{\circ}C$	$0.25 \pm 0.01\,^{\circ}C$
	After 50	$0.23 \pm 0.05\,^{\circ}C$	$0.23 \pm 0.07\,^{\circ}C$
Left–right eye corneal temperature difference	Below 30	$0.23 \pm 0.21\,^{\circ}C$	$0.17 \pm 0.13\,^{\circ}C$
	30–50	$0.26 \pm 0.27\,^{\circ}C$	$0.25 \pm 0.19\,^{\circ}C$
	After 50	$0.23 \pm 0.1\,^{\circ}C$	$0.23 \pm 0.24\,^{\circ}C$

In summary, Eq. (18) calculates the average difference in between the minimum temperature obtained using automated method and the minimum temperature acquired using manual method of all corneas. Eq. (19) calculates the average difference in between the maximum temperature obtained using those two methods.

4. Results

Table 2 illustrates some basic statistical parameters evaluated from thermograms of subjects of different age groups analyzed using automated and manual localization of cornea. Values obtained for average corneal temperature of both methods were close to each other, $34.01 \pm 0.64\,^{\circ}C$ for automated localization and $33.99 \pm 0.63\,^{\circ}C$ for manual localization. The dispersion of temperatures within a single cornea is represented by the mean and standard deviation within localized cornea. It can be seen from Table 2, that the average temperature for both automated and manual corneal localization methods gave similar results. However in the case of age group below 30 years, the automated method gave a slightly higher value as compared to manual method, as shown in Table 3.

The values reported are in the form of "mean value $\pm$ standard deviation". As there is no widely accepted population mean for ocular surface temperature, and hence we did not perform hypothesis test on mean. Also, we did not consider the value acquired by manual method as population mean, so we did not perform any test against values obtained through manual method. In this case, there would be no statistical analysis performed on confidence limits on the mean, and hence no confidence interval and confidence level acquired in this study. However, we did perform statistical analysis on the hypothesis H_0: $\mu_A - \mu_M = 0$ for all the reported results, where A denotes the automated method and M the manual method. At the level of significance of 95%, we failed to reject the hypothesis for all results.

Fig. 7 presents the distributions of average corneal temperature acquired using methods of automated and manual corneal localization. Fig. 8 shows the distributions of left–right eye average corneal temperature difference on methods of both automated and manual corneal localization. Similar trends in these distributions on both methods were observed, as shown in the figures.

Average corneal surface temperature versus age on both corneal localization methods were plotted in Fig. 9. Results from linear regression on both methods showed a downward trend, i.e. average corneal surface temperature decreased as age of subject increased. However, it was found that in both methods such correlation was not very significant ($R^2 = 0.08$ and $R^2 = 0.07$ respectively for automated and manual methods).

5. Discussion

In this study both the automated and manual corneal localization methods were employed to study ocular surface temperature. OST has been studied using a number of ways in the past, and the way of delineation of circular cornea were proposed recently [8,9]. However, in these studies the diameters of the delineated circular cornea were actually smaller compared to the diameters of the actual cornea in most cases. Hence, the result of these analyses may not exactly reflect the actual temperature within the cornea.

Though there were reports demonstrating possibilities of using OST to diagnose ocular disease, but only one report has actually made use of OST to do it. In that study, the researchers diagnosed dry eye from sequence of ocular thermograms, with a sensitivity of 79.3% and a specificity of 75% [24]. They manually located the region of interest, which is an encircled region 4.4 mm diameter (22 pixels) positioned at the eye center. The manual method adopted in this paper has more

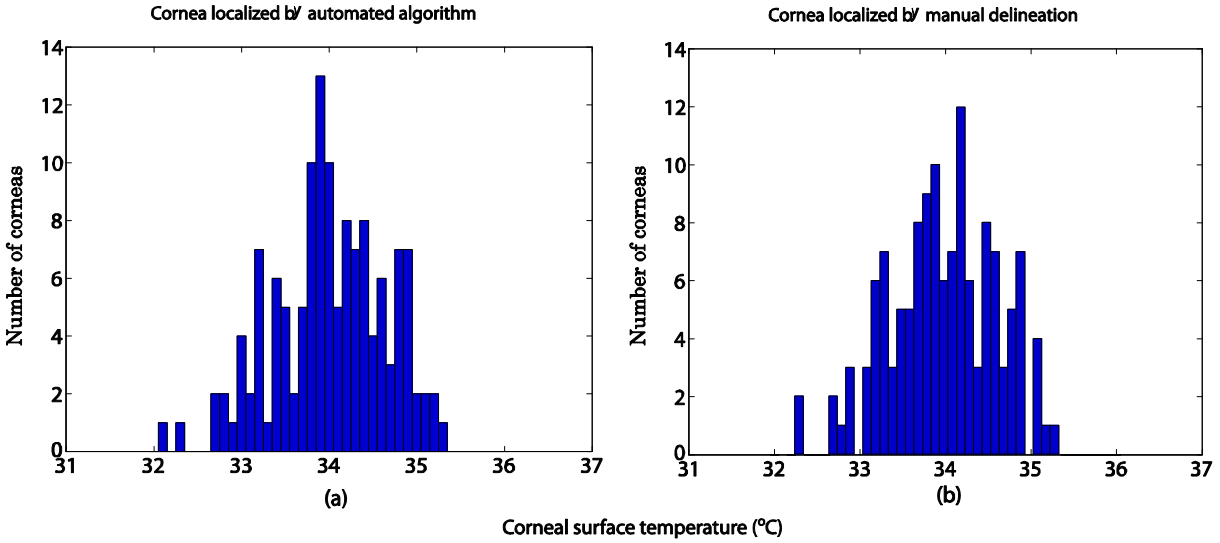

Fig. 7. Distribution of average corneal surface temperature versus number of corneas on methods of (a) automated and (b) manual corneal localization.

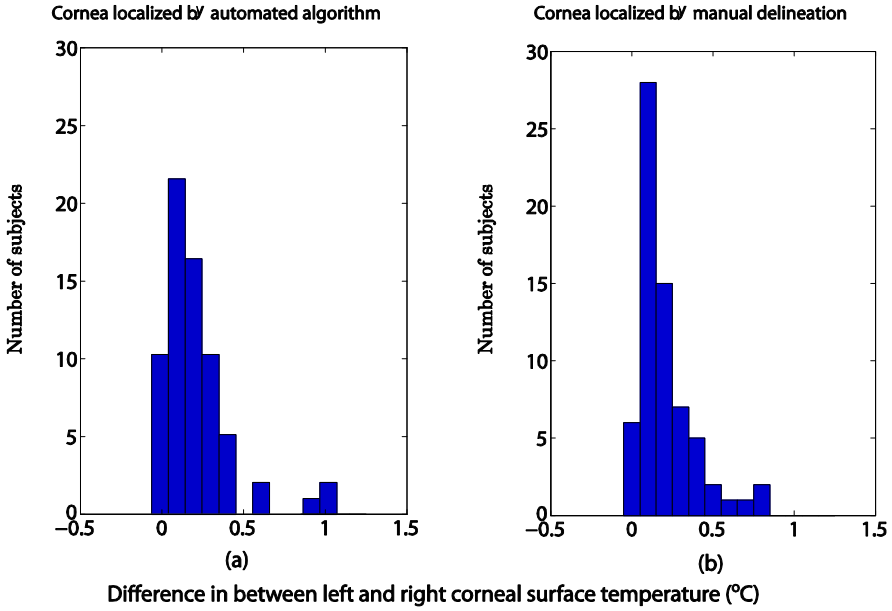

Fig. 8. Distribution of interocular difference (left–right) in corneal surface temperature versus number of subjects on methods of (a) automated and (b) manual corneal localization.

consistency and less ambiguity compared to their method, as discussed in [25]. Therefore, we pick up our manual method as a reference of comparison with the automated method.

The proposed algorithm in localizing eye and cornea was reported to have a success rate of 90% [17,18]. In most cases, this automated algorithm (including localization of eye, removal of eye lashes and thermogram analysis) took less than 2 minutes (on a PC having Intel core duo) to complete the analysis. The current proposed target tracing function (Eq. (7)) helps in the automatic localization of eye without any human intervention in the initialization and monitoring of snake convergence, a step often required in many snake applications.

It can be understood from Table 2 and Table 3, that the results given by both methods were very close to each other (NRMSE % is very low). This showed that our proposed automated algorithm can be used as a substitute for the manual method in studying corneal temperature. This automated algorithm can also be used for applications such as computer-based diagnostic tool to detect the different ocular diseases.

For ocular thermogram, there is often no distinguishable orientation pattern in the region of anterior surface. To detect eyelashes, we need to generate distinguishable orientation pattern and hence we superimposed dark–bright alternating circular strips on the square matrix. In most cases, temperatures of eyelashes (both isolated and grouped) are far lower

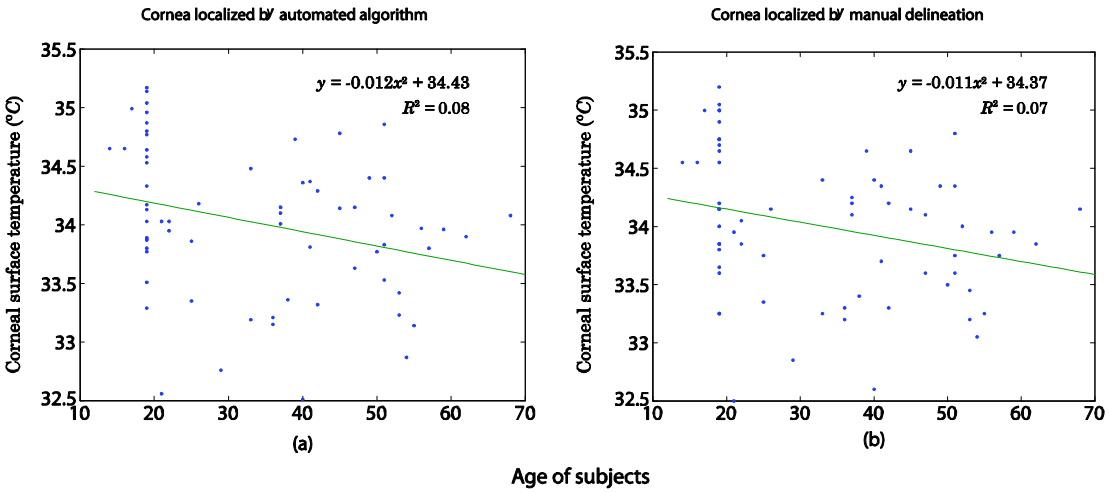

Fig. 9. Average corneal surface temperature versus age on both corneal localization methods.

compared to anterior surface, in ocular thermogram these are manifested as darker pixels. These pixels are so dark such that even with the superimposed circular strips, these regions still do not have distinguishable orientation pattern compared to the other region.

The square matrix acquired after ocular localization is at first resized to a standard size of 300×300 in the removal of eyelashes, as different subjects have different size of eye, and to prevent the width of the later superimposed circular strip to be too small (less than 1 pixel). At current setting, the block size is 6×6 pixels, and the width of circular strip is 2.8 pixels. The superimposed circular strips are observed to have virtually no effect on the eyelashes region. And the processing block contains only small part of eyelashes, so when a processing block falls on a part of eyelashes, it has no specific orientation pattern. In regions other than eyelashes, each of the corresponding blocks will usually contain one bright and one dark strip, giving specific orientation in that block, and one of the 8 Gabor filters would respond and return greater value (in terms of absolute value); in this case, the standard deviation acquired based on the response of these 8 filters would also be greater. On the contrary, for a block (block contains eyelashes) that does not have a specific orientation, the 8 Gabor filters would return similar value and the standard deviation acquired would be small.

Though there are some minor differences in values acquired by manual and automated methods (the values are reported up to two decimal places to illustrate such minor dissimilarity, otherwise many results would be seen equal), the effect of eyelash removal was not clearly seen within Tables 2 and 3, nor in Figs. 7, 8 and 9. However, from Eqs. (6) and (7), one can see its effect and its importance. D_{Mn} calculated for this study was 0.62, and D_{Mx} is 0.18. It showed that there was not much difference in the maximum temperature obtained in between the automated and manual corneal localization methods. But the eyelash removal algorithm, has prevented substantially lower temperatures of eyelashes to be read in as part of the corneal surface temperature, and hence lead to a comparatively large D_{Mn}.

The mean of OST in this study was 34.01 °C, 0.79 °C lower than the mean reported by the study of Mapstone for 70 subjects [6], and 0.29 °C lower than the temperature of geometric center of cornea reported by the study of Efron et al. [10]. Girardin et al. have reported average corneal temperature of 33.7 °C for 266 subjects, but the corneal temperature was not studied [26]. Exact measurement of temperature on limbus was not performed in this study, instead, standard deviation of temperatures was calculated to give a view on the temperature variation over the region of interest (it is 0.24 °C). The mean interocular difference in OST was found to be 0.22 °C. And there were 3% subjects having interocular difference in corneal surface temperature exceeding 0.75 °C, which was similar to the result reported in [11].

It was reported that corneal surface temperature reduced with an increase in age [27]. However Morgan et al. have shown that subject's age was not a good predictor of central corneal surface temperature [12]. In our present work, there was no significant correlation in between corneal surface temperature and age ($R^2 = 0.08$) and -0.012 °C per year, which were similar to $R^2 = 0.08$ and -0.01 °C per year by Morgan et al. [12].

6. Conclusion

Thermography can be used to study the ocular surface temperature (OST), for possible diagnosis of different ocular diseases. In this work the performance of an automated and manual corneal localization methods was compared to study OST. Our results show that the proposed automated algorithm is simple and easy to use. The accuracy in the localization of eye and cornea is as effective as the manual method. The average corneal surface temperature is 34.01 °C, and with no significant correlation between the corneal surface temperature and age.

References

[1] E.F.J. Ring, Progress in the measurement of human body temperature, IEEE Eng. Med. Biol. Mag. 17 (1998) 19–24.
[2] E.Y.K. Ng, Y. Chen, Segmentation of breast thermogram: improved boundary detection with modified snake algorithm, J. Mech. Biol. 6 (2006) 123–136.
[3] T.K. Kalili, B.M. Gratt, Electronic thermography for the assessment of acute temporomandibular joint pain, Compend. Contin. Educ. Dent. (1996) 979–983.
[4] A. Merla, G.L. Romani, A. Tangherlini, S.D. Romualdo, M. Proietti, E. Rosato, A. Aversa, F. Salsano, Penile cutaneous temperature in systemic sclerosis: a thermal imaging study, Int. J. Immunopathol. Pharmacol. 20 (2007) 139–144.
[5] A. Holmberg, The temperature of the eye during application of hot packs and after milk injections, Acta Ophthalmol. (Copenhagen) 30 (1952) 347–364.
[6] R. Mapstone, Measurement of corneal temperature, Exp. Eye Res. 7 (1968) 237–243.
[7] C. Purslow, J.S. Wolffsohn, Ocular surface temperature, a review, Eye Contact Lens 31 (2005) 117–123.
[8] U.R. Acharya, E.Y.K. Ng, G. Yee, T. Hua, M. Kagathi, Analysis of normal human eye with different age groups using infrared images, J. Med. Syst. 33 (2009) 207–213.
[9] E.Y.K. Ng, J.H. Tan, E.H. Ooi, C. Chee, U.R. Acharya, Variations of ocular surface temperature with different age groups, in: Image Modeling of Human Eye, Artech House, 2008.
[10] N. Efron, G. Young, N. Brennan, Ocular surface temperature, Curr. Eye Res. 8 (1989) 901–906.
[11] P.B. Morgan, M.P. Soh, N. Efron, A.B. Tullo, Potential applications of ocular thermography, Optometry Vision Sci. 70 (1993) 568–576.
[12] P.B. Morgan, M.P. Soh, N. Efron, Corneal surface temperature decrease with age, Contact Lens Anterior Eye 22 (1999) 11–13.
[13] C. Purslow, J.S. Wolffsohn, J. Santodomingo-Rubido, The effect of contact lens wear on dynamic ocular surface temperature, Contact Lens Anterior Eye (2005) 29–36.
[14] R. Mapstone, Determinants of corneal temperature, Br. J. Ophthalmol. 52 (1968) 729–741.
[15] R. Mapstone, Corneal thermal patterns in anterior uveitis, Br. J. Ophthalmol. 52 (1968) 917–921.
[16] S. Petrou-Binder, Thermotopography shows 'enormous promise' for diagnosis and treatment of eye diseases, http://www.escrs.org/eurotimes/march2003/thermo.asp, last accessed 5 April 2010.
[17] J.H. Tan, E.Y.K. Ng, U.R. Acharya, Detection of eye and cornea on IR thermogram using genetic snake algorithm, in: 9th International Conference on Quantitative Infrared Thermography, Krakow, Poland, 2008, pp. 143–150.
[18] J.H. Tan, E.Y.K. Ng, U.R. Acharya, Automated detection of eye and cornea on infrared thermogram using snake and target tracing function coupled with genetic algorithm, Quant. Infrared Thermogr. Int. J., in press.
[19] M. Kass, A. Witkin, D. Terzopoulos, Snakes: active contour models, Int. J. Comput. Vision (1988) 321–331.
[20] C. Xu, J.L. Prince, Snakes, shapes, and gradient vector flow, IEEE Trans. Image Process. 7 (1998) 359–369.
[21] A.L. Yuille, D.S. Cohen, P.W. Hallinan, Feature extraction from faces using deformable templates, in: Proceedings CVPR'89, IEEE Computer Society Conference, San Diego, CA, USA, 1989, pp. 104–109.
[22] D. Alonso-Caneiro, D.R. Iskander, M.J. Collins, Estimating corneal surface topography in videokeratoscopy in the presence of strong signal interference, IEEE Trans. Biomed. Eng. 55 (2008) 2381–2387.
[23] T.K. Moon, The expectation-maximization algorithm, IEEE Signal Process. Mag. 13 (1996) 47–60.
[24] H.K. Chiang, C.Y. Chen, H.Y. Cheng, K.-H. Chen, D.O. Chang, Development of Infrared Thermal Imager for Dry Eye Diagnosis, Proceedings of SPIE, The International Society for Optical Engineering, San Diego, CA, USA, 2006.
[25] J.H. Tan, E.Y.K. Ng, U.R. Acharya, C. Chee, Infrared thermography on ocular surface temperature: a review, Infrared Phys. Technol. 52 (2009) 97–108.
[26] F. Girardin, S. Orgül, C. Erb, J. Flammer, Relationship between corneal temperature and finger temperature, Arch. Ophthalmol. 117 (2007) 166–169.
[27] J. Alio, M. Padron, Influence of age on the temperature of the anterior segment of the eye, Ophthalm. Res. 14 (1982) 153–159.

Jen-Hong Tan is currently a Ph.D. student in Nanyang Technological University, Singapore, under Assoc. Prof. E.Y.K. Ng since 2006. He received his Bachelor of Engineering from Nanyang Technological University. His major interest is in biomedical signal processing.

E.Y.K. Ng received Ph.D. at Cambridge University with a Commonwealth Scholarship. His main area of research is thermal imaging, human physiology, biomedical engineering; computational turbomachinery aerodynamics; microscale cooling problems; CFD. He is an adjunct National University Hospital Scientist in Singapore. He has published more than 300 papers in refereed international journals (200), international conference proceedings (70), textbook chapters (30) and others (22). Eddie is co-Editor-in-Chief for the Journal of Mechanics in Medicine and Biology; Assoc. Editor for Int. Journal of Rotating Machinery; Computational Fluid Dynamics Journal (CFD); member of Editorial Board for Chinese Journal of Medicine, Journal of Biomedical Science and Engineering, Journal of Healthcare Engineering, Open Medical Informatics Journal, The Open Numerical Methods Journal, World Journal of Clinical Oncology, and co-chairman for 15th Int. Conf. on Mechanics in Medicine and Biology (2006). Ng is an invited speaker for many international scientific conferences/workshops. Recently, he has co-edited 5 books: "Cardiac Pumping and Perfusion Engineering" by WSPC Press (2007); "Imaging and Modelling of Human Eye" by Artech House (2008); "Distributed Diagnosis and Home Healthcare" by ASP (2009); "Performance Evaluation in Breast Imaging, Tumor Detection and Analysis" by ASP (2010) and "Computational Analysis of Human Eye with Applications" by WSPC Press (in press). Also, he co-authored a text book: "Compressor Instability with Integral Methods" by Springer (2007). More details are available at http://www3.ntu.edu.sg/home/mykng/.

Rajendra Acharya U is a visiting faculty in Ngee Ann Polytechnic, Singapore and adjunct faculty in Manipal Institute of Technology, Manipal, India. He received his Ph.D. from National Institute of Technology Karnataka, Surathkal, India and DEngg from Chiba University, Japan. He has published more than 125 technical papers (95 international journals and 30 international conferences) and four books. His major interests are in biomedical signal processing, bio-imaging, data mining, visualization and biophysics for better healthcare design, delivery and therapy.